AIAA JOURNAL
Vol. 48, No. 10, October 2010

Surface-Pressure Fluctuations from Separated Flow over an Axisymmetric Bump

Gwibo Byun* and Roger L. Simpson†
Virginia Polytechnic Institute and State University, Blacksburg, Virginia 24061

DOI: 10.2514/1.J050429

Surface-pressure fluctuations are measured for the separated flow over a smoothly contoured axisymmetric bump or hill with an approaching two-dimensional turbulent boundary-layer thickness that is half of the bump height and momentum thickness Reynolds number $Re_\theta = 7,300$. Two piezoresistive pressure transducers were used to measure the pressure fluctuations and to remove the noise by the subtraction method. The flow over this bump shows highly unsteady saddle-focus separations on the leeside curved surface. The magnitude of surface-pressure fluctuations is higher on the leeside than the windward side. The power spectral levels of pressure fluctuations are high in the low-frequency region, and they contribute dominantly to the resulting surface-pressure fluctuation on the leeside. In the separated region, large-scaled eddy structures associated with the streamwise vortices emanated from three-dimensional separations are major sources for the pressure fluctuation generation, and the rapid spectral decay is observed. From the approximate analysis, the asymmetric negative skewed histogram of surface-pressure fluctuations appears in the separated region.

Nomenclature

a	=	radius of the bump base, m
C_P	=	mean pressure coefficient, $(\bar{p} - \bar{p}_{\text{ref}})/q_{\text{ref}}$
d^+	=	nondimensional pressure transducer sensing diameter, du_τ/ν
f	=	frequency, Hz
H	=	bump height, m
I_0	=	modified Bessel function of the first kind
J_0	=	Bessel function of the first kind
p'	=	pressure fluctuation at the model surface, Pa
q_{ref}	=	dynamics pressure of freestream, $\frac{1}{2}\rho U_{\text{ref}}^2$, Pa
Re_θ	=	momentum thickness Reynolds number, $U_{\text{ref}}\theta/\nu$
r	=	local horizontal radius of bump in x, z plane, m
S_P	=	skewness of p' probability density function, $\overline{p'^3}/(\overline{p'^2})^{3/2}$
St	=	Strouhal number, fH/U_{ref}
U, V, W	=	instantaneous velocities in the x, y, and z directions, respectively, m/s
$\bar{U}$, $\bar{V}$, $\bar{W}$	=	mean velocities in the x, y, and z directions, respectively, m/s
U_C	=	convection velocity, m/s
U_{ref}	=	reference freestream velocity upstream of bump, m/s
$-\overline{uv}$, $-\overline{uw}$, $-\overline{vw}$	=	kinematic Reynolds shear stresses, m^2/s^2
u_τ	=	friction velocity, $\sqrt{\tau_w/\rho}$, m/s
$\overline{u^2}$, $\overline{v^2}$, $\overline{w^2}$	=	kinematic Reynolds normal stresses, m^2/s^2
u', v', w'	=	velocity fluctuations in the x, y, and z directions, respectively, m/s
x	=	streamwise direction in tunnel coordinate, m
y	=	vertical direction in tunnel coordinate, m
y_{L0}^+	=	nondimensional distance from bump surface normalized by two-dimensional turbulent boundary layer u_τ
z	=	spanwise direction in tunnel coordinate, m
δ	=	upstream boundary-layer thickness, m
γ^2	=	coherence function of surface-pressure fluctuation, $\gamma^2 = \lvert\Phi_{p'_1p'_2}\rvert^2/\Phi_{p'_1}\Phi_{p'_2}$
θ	=	phase angle function of surface-pressure fluctuation, $\theta = (2\pi f\Delta x)/U_C$
μ	=	mean of random variable
ν	=	kinematic viscosity of flow, m^2/s
ρ	=	mass density of flow, kg/m^3
σ	=	standard deviation of random variable
τ_W	=	local wall shear stress, Pa
Φ	=	power spectrum of surface-pressure fluctuation, $\text{pa}^2 \cdot \text{s}$, $\overline{p'^2} = \int_0^\infty \Phi(f)\,\mathrm{d}f$
ψ	=	yaw angle, deg

Subscripts

L	=	quantities in local surface-aligned right-hand coordinate system
2D	=	quantities based on undisturbed two-dimensional turbulent boundary layer

I. Introduction

THE turbulent surface-pressure fluctuations beneath a turbulent shear flow are a result of the velocity fluctuations of turbulent structures. The pressure fluctuation structure is a source of flow-induced noise and vibration of solid bodies, which are of concern for many engineering applications. Therefore, much research on wall-pressure fluctuations beneath a turbulent boundary layer has been conducted, and Bull [1] has provided a review of statistical and theoretical descriptions and the frequency spectral scaling behavior. However, most of those investigations are equilibrium or separated two-dimensional (2-D) boundary layers. Much research has been conducted to understand the dynamics of flow over blunt bodies, such as the cube, circular cylinder, and sphere, but with inadequate information about surface-pressure fluctuations and velocity fluctuations of turbulence near the surface.

However, many practical cases are three-dimensional (3-D) flows that may involve mean vortices. Goody and Simpson [2] and Goody et al. [3] have provided detailed surface-pressure fluctuation data for two well-documented 3-D flowfields with mean separation vortices.

Presented as Paper 2010-0007 at the 48th AIAA Aerospace Sciences Meeting, Orlando, FL, 4–7 January 2010; received 12 January 2010; revision received 5 May 2010; accepted for publication 7 May 2010.

*Postdoctoral Associate, Department of Aerospace and Ocean Engineering, 215 Randolph Hall. Member AIAA.

†Jack E. Cowling Professor, Department of Aerospace and Ocean Engineering, 215 Randolph Hall. Fellow AIAA.

In spite of current computational ability and capabilities for large-eddy simulation (LES), few investigations of separated turbulent flow over a 3-D body include the surface-pressure fluctuation behavior. Therefore, the structure and physics of surface-pressure fluctuations, as related to the turbulent flowfield (especially for high Reynolds numbers and 3-D complex flows) are still not completely described. Complex flow-induced pressure fluctuations are difficult to model. Therefore, it is necessary to investigate the characteristics of surface-pressure fluctuations along with extensive turbulent velocity field measurements for complex flows.

For the present paper, the surface-pressure fluctuations produced by the flow over a smoothly contoured 3-D asymmetric bump or hill are considered. The detailed vortical separated turbulent flowfield has been measured and discussed by the current authors [4–7]. This flow features complex 3-D vortical separations that occur on the leeside of the bump and merge into large streamwise mean vortices downstream. Figure 1 illustrates the near-surface flow structure over this bump. Mean flow 3-D separations (dashed lines in Fig. 1b) occur on the leeside, with one saddle separation on the centerline that is connected by a separation line to one focus separation on each side of the centerline. Downstream of the saddle point, the mean backflow converges to the focal separation points in a thin region confined within about 0.15δ from the local bump surface. The mean backflow zone (gray in Fig. 1b) is supplied by the large eddies (solid lines in Fig. 1b) with intermittently forward and backward flow, as well as by the near-surface flow from the side of the bump. The separated flow has a higher turbulent kinetic energy (TKE) and shows bimodal velocity probability histograms in local surface tangent coordinates U_L and W_L, which appear to be due to highly unsteady turbulent motions. By the mode-averaged analysis of bimodal histograms [7], highly unsteady low-frequency flow structures are estimated, and unsteady 3-D separations seem to occur over a wide spatial region on the bump leeside, with a large intermittent attached and detached flow region, which is varying in time. These bimodal features with highly correlated local u'_L and w'_L motions are the major source of large Reynolds stresses $\overline{u'_L{}^2}$, $\overline{w'_L{}^2}$, and $-\overline{u'w'}_L$ [7]. Because of the variation of the mean flow angle in the separation zones, the turbulent flow from different directions is noncorrelated, resulting in lower shearing stresses. Farther from the wall, large streamwise vortices form from flow around the sides of the bump. At the downstream wake plane, the vortices in the outer region produce large turbulence levels near the centerline and appear to have low-frequency motions that contribute to turbulent diffusion.

This specific bump flow has been used as an international test case for many computational fluid dynamics (CFD) researchers in order to develop turbulent models of turbulent separated flow on a 3-D curved surface [8–13]. Although their intensive efforts have resulted in qualitative and quantitative model improvements, there is no information regarding the pressure fluctuations on the bump surface. Therefore, the major goals of the current study are to investigate the characteristics of surface-pressure fluctuations produced by a well-documented nonequilibrium 3-D separated turbulent flow on a

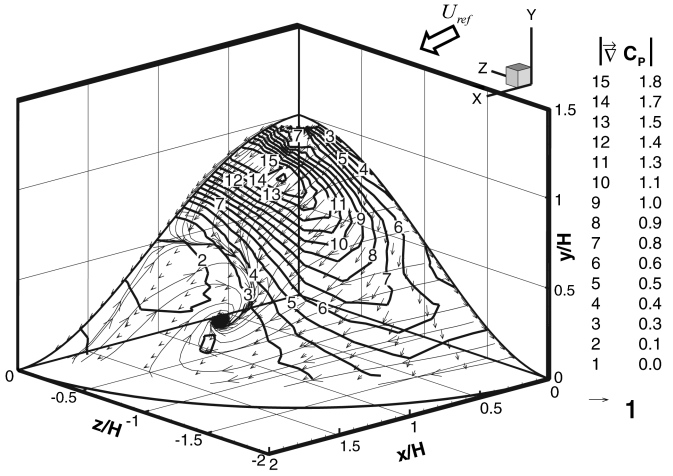

a) Surface-pressure gradient magnitude contour (bold lines), its vectors given by arrows and thin lines connecting $\overline{U}_L i_L + \overline{W}_L k_L$ vectors locally tangent to surface at $y+_{L0} = 11$

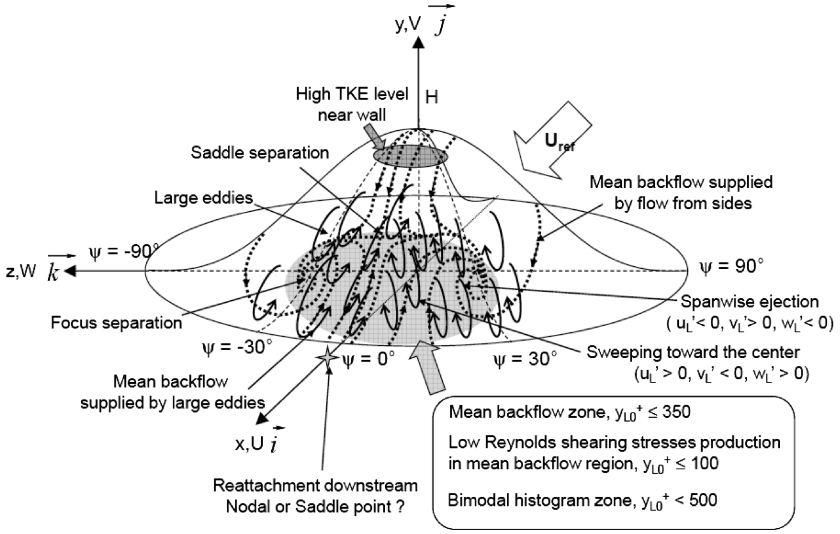

b) Flow structures on leeside of bump

Fig. 1 Near-wall flowfield and flow structures over bump [6].

curved surface, which is of practical engineering interest, and to provide a reference case for modeling.

II. Experimental Apparatus, Techniques, and Uncertainties

A. Facilities, Bump, and Measurement Techniques

The pressure fluctuation measurements were conducted in the Virginia Polytechnic Institute and State University low-speed boundary-layer wind tunnel, which has been used in much previous bump work [4–7]. At a nominal speed of $U_\infty = 27.5$ m/s and a temperature of 25 ± 1°C, the turbulence intensity in the tunnel freestream was 0.1%, and the potential core was uniform to within 0.5% in the spanwise and 1% in the vertical directions. When the bump was not in place, a mean 2-D zero pressure gradient turbulent boundary layer (2DTBL) was present with $\delta = 39$ mm and $Re_\theta = 7,300$. The bump was mounted in the floor center of the 0.91-m-wide, 0.25-m-high, and 7.62-m-long test section, 3 m from the test-section leading edge. The smoothly machined axisymmetric shape shown in Fig. 1 was selected by naval architects to have smooth variations of surface curvature that are defined by Eq. (1)

$$\frac{y(r)}{H} = -\frac{1}{6.04844}\left[J_0(\Lambda)I_0\left(\Lambda\frac{r}{a}\right) - I_0(\Lambda)J_0\left(\Lambda\frac{r}{a}\right)\right] \quad (1)$$

where $\Lambda = 3.1962$ and $H = 78$ mm $= 2\delta$ are the height of the bump, and $a = 2H$ is the radius of the circular base of the bump. Here, J_0 is the Bessel function of the first kind, and I_0 is a modified Bessel function of the first kind.

Endevco 8507-C2 piezoresistive pressure transducers were used. They are a circular deflection type and have a flat frequency response up to 70 kHz and about a 2 mm sensing diameter. The transducer was mounted inside the bump and measured pressure fluctuations through a 0.5-mm-diam pinhole. Both the pinholes and the transducer were located perpendicular to the local bump surface. The resonant frequency due to the pinhole and associated transducer housing is about 11–12 kHz, and the frequency response is close to Goody's calibration of the same transducer, pinhole diameter and housing volume [14]. Therefore, the resonance and related spectral response were corrected by his second-order frequency transfer function.

The transducer signal was amplified by a strain gauge signal conditioning amplifier (Vishay Measurements Group model 2310) and 256 segments, with 32,768 samples per segment, were acquired at a 50 kHz sampling rate with a 14-bit digitizer (ZTEC Instruments, ZT410PCI-21). The power spectrum of each segment fast Fourier transform was frequency-bin-averaged to get a final one-sided spectrum. The total sampling period at each location was about 3 min, which is much longer than 200 times the integral time scale corresponding to the largest eddies [7]. Thus, this record time produced ergodic statistics of p' contributions from all relevant turbulent motions over the bump.

To extract the turbulent boundary-layer contributions to p' from p' that contain contributions due to other sources, such as coherent acoustic pressure fluctuations and external vibrations generated by the facility, two transducer signals were subtracted, using the technique described by Simpson et al. [15] and McGrath and Simpson [16]. As shown in Fig. 2, one transducer was mounted on the bump surface and the other was apart spanwise, at least 2.6δ on the flat plate. Therefore, it is assumed that the individual largest-scale bump-generated motions are not correlated in the spanwise direction to one another over this distance. In addition, the freestream facility-related acoustic and vibrational contribution to pressure fluctuations must be correlated to one another at different spanwise locations, so subtraction of the signals from the two transducers when they are located at the same streamwise location should eliminate these coherent signals. Under these conditions, the proper p' on the bump surface due to turbulence can be obtained from noise-contaminated signals. Figure 2 show the schematic view of the apparatus.

B. Measurement Uncertainties

The uncertainties of $\overline{p'^2}$ and p' are calculated following the analysis of Goody [14]. The statistical convergence uncertainty of the spectral power of 256 averaged ensembles for the present study is estimated to be $\pm 6.3\%$. The maximum deviation of the spectral power due to the finite resolution of pinhole-pressure transducer housing is estimated to be $\pm 12\%$ within the frequency range of interest by Corcos's analysis [17]. It is noted that the nondimensional pressure transducer sensing diameter based on the approaching 2DTBL u_τ is $d^+ = 26$ for the current measurements. Therefore, the combined uncertainty of spectral power is estimated to be $\pm 13.5\%$. Since $\overline{p'^2}$ values are calculated by the numerical integration of the power spectrum density (PSD) of p', the combined uncertainty of the preceding spectral power values is also integrated in order to estimate the uncertainties of $\overline{p'^2}$. Following the analysis of Kline and McClintock [18], the uncertainty of $\overline{p'^2}$ is $\pm 10\%$.

III. Results and Discussion

A. Two-Dimensional Zero Pressure Gradient Turbulent Boundary-Layer Surface p' Power Spectrum Density

To verify the microphone, housing, and pinhole behavior observed by Goody [14], a nominal zero pressure gradient flat plate 2DTBL p'

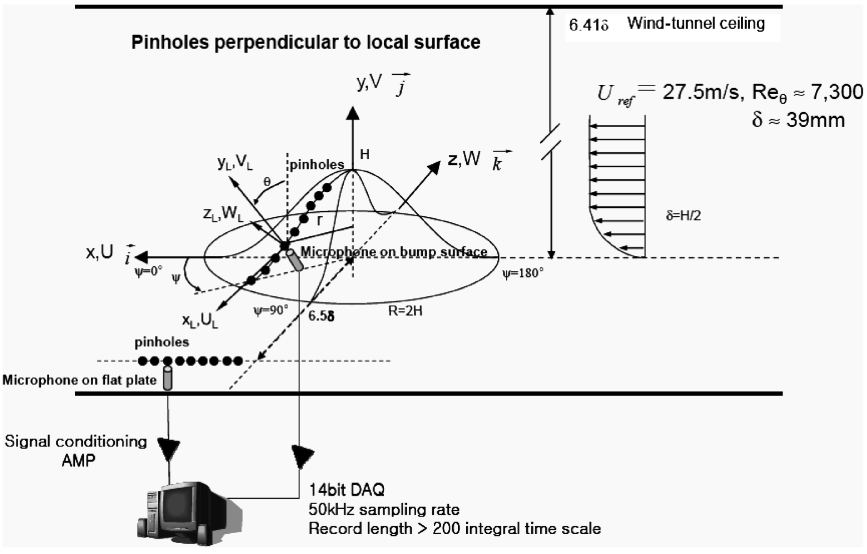

Fig. 2 Schematic view of experimental apparatus for surface-pressure fluctuation measurements on the bump, tunnel coordinates (x, y, z),and local coordinates(x_L, y_L, z_L) (AMP denotes amplifier, and DAQ denotes data acquisition).

PSD was measured without the bump and compared with Goody's result at the same Re_θ in Fig. 3. The two microphones were 70 mm($\approx 1.8\delta$) spanwise apart, and the noise cancellation technique described previously was applied. The present p' PSD agrees well with Goody's spectrum, indicating proper noise removal technique and enough spatial resolution of pinhole for the high frequency range. It varies as f^{-5} dependence in the high frequency region, which is associated with the small-eddy structure in the sublayer. Note that Goody used only one pressure transducer with a time-delay noise cancellation technique that assumes periodic low-frequency unsteadiness and wind-tunnel interference. The subtraction method for the present data is more effective on the noise cancellation for low frequencies below $f \approx 260$ Hz ($2\pi f\delta/u_\tau \approx 64$), where the spectral peak is observed because both microphones detect all of the same unsteadiness and wind-tunnel interference. The p' spectrum varies about as $f^{0.5}$ dependence for 40 Hz $\leq f \leq$ 260 Hz, showing the decay of the contribution of large-scale motions in a outer layer to the pressure fluctuation. However, it does not vary as the sometimes observed f^2 below $f \approx 20$ Hz ($2\pi f\delta/u_\tau \approx 5$)[1] but it shows almost a flat level, which represents a background noise. The p' spectrum shows an $f^{-0.8}$ dependence in the midfrequency region, although Bradshaw [19] argued that the p' spectrum has an f^{-1} dependence in this frequency range, associated with the overlap region of a 2DTBL for high Reynolds numbers. Some variations of a power law decay, $f^{-0.7} \sim f^{-1}$, have been observed in a lower Reynolds number range [14–16,20–22]. The $\sqrt{\overline{p'^2}}/q_{\text{ref}}$ and $\sqrt{\overline{p'^2}}/(\tau_W)_{2D}$ are 0.008 and 3.32 for the 2DTBL, respectively, from integration of p' PSD, which are consistent with Goody's 2DTBL ($Re_\theta \approx 7300$) result, 0.009 and 3.44 [2].

B. Bump Surface p'

The bump surface locations for pressure fluctuation measurement are shown in Fig. 2 and Table. 1. There are nine locations from the top, along the bump radius, for the microphone location; the bump was rotated from $0 \sim 90°$ about the y axis (ψ) for the leeside measurements and at $\psi = 120$, 150, and 180° on the windward side. The second microphone was located spanwise at the same streamwise location on the flat plate as the bump microphone (Fig. 2). The present measurements are focused on the bump leeside, where the vortical separations occur.

The pressure coefficient C_P and rms values of p' along the centerline are shown in Fig. 4. Note that the bump frontal area is 5.0% of the test-section cross-sectional area, and the tunnel sidewall inserts were used to minimize blockage-induced pressure gradients around the bump. The p' rms values are normalized by $q_{\text{ref}} = 415.9$ Pa and $(\tau_W)_{2D} = 1.014$ Pa, which are constant. The p' magnitudes on the windward side are much lower than those in the leeside due to the favorable pressure gradient and the flow acceleration on the

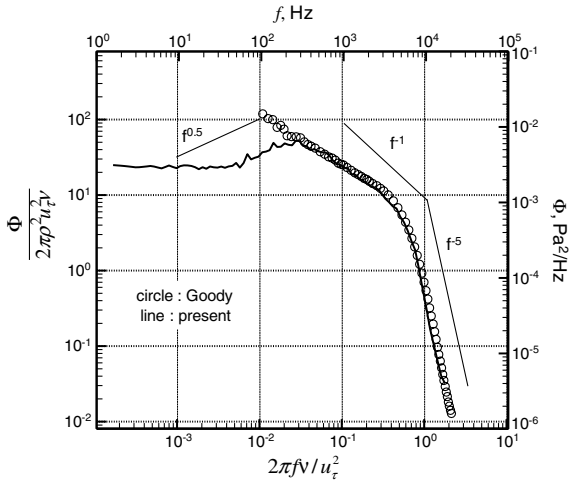

Fig. 3 p' PSD of 2DTBL ($Re_\theta \approx 7300$) compared with data of Goody [14].

Table 1 Locations for p' measurement on bump surface

	Yaw, deg	
r/H	Leeward side	Windward side
0.254	0, 10, 20, 30, 40, 50, 90	120, 150, 180
0.496	0, 10, 20, 30, 40, 50	——
0.706	0, 10, 20, 30, 40, 50, 60, 90	120, 150, 180
0.91	0, 10, 20, 30, 40, 50, 60	——
1.044	0, 10, 20, 30, 40, 50, 60, 90	120, 150, 180
1.244	0, 10, 20, 30, 40, 50	——
1.386	0, 10, 20, 30, 40, 50, 60	——
1.615	0, 10, 20, 30, 40, 50, 90	120, 150, 180
1.853	0, 10, 20, 30, 40, 50, 60, 90	——

windward side [4]. Although there are not many measured locations, the magnitude of p' on the windward side decreases toward the top and begins to increase after the bump apex under the adverse pressure gradient. Further downstream from the top, the p' magnitude shows a drop at $x/H = 0.706$, which is upstream from the saddle separation and increases further downstream from $x/H = 0.706$. Figure 5 shows the contour of normalized p' on the bump leeside. The thin solid lines indicate the near-wall mean flow pattern tangent to the wall [6]. Byun and Simpson [6] reported the saddle-focus separation and the mean backflow region downstream from $x/H \approx 0.96$ on the leeside centerline. High p' magnitudes occur near the top, $x/H = 0.3 \sim 0.5$ and $|z/H| \leq 0.5$, where the highest adverse pressure gradient was observed [4] and the mean backflow region near the focus. Considering the flow structures on the bump leeside [6,7], the large eddies that are related to the vortices that emanate from the separations are the dominant source of p' in the mean backflow region and are discussed later with the spectral features. For $x/H = 0.3 \sim 0.5$ and $|z/H| \leq 0.5$, the high p' magnitudes are related to the large vorticity flux generated by the high adverse mean pressure gradient and the highest TKE production in this region [7,13]. The magnitude drop at $x/H = 0.706$ may be related to the beginning of separation near the intermittent transitory detachment (ITD), defined as the 20% fraction of time of the instantaneous backflow [23], which is observed near the wall ($y^+_{L0} \approx 14$) at this location [6]. It also should be noted that the saddle-focus separation is highly unsteady and appears in a wide leeside region. The p' magnitude increases toward

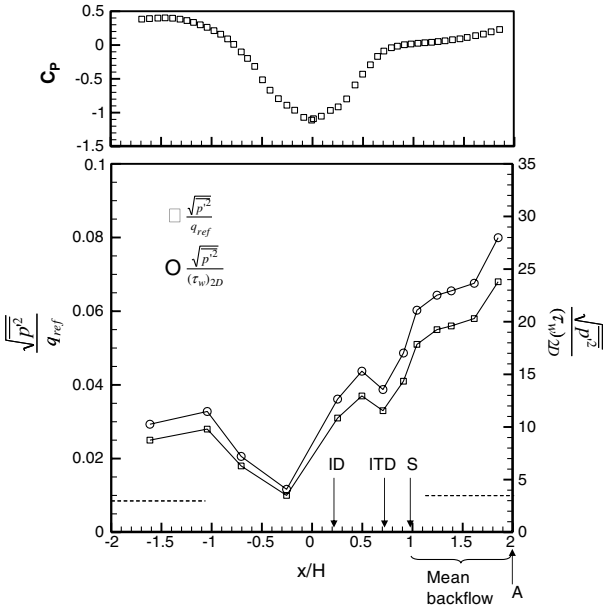

Fig. 4 C_P [4] and normalized p' rms along the centerline. Dashed lines denote the level for the 2DTBL. ID, ITD, S, and A are locations of incipient detachment (1% instantaneous backflow), ITD (20% instantaneous backflow), separation (detachment; 50% instantaneous backflow), and reattachment.

$x/H = 2.0$, where flow reattachment is expected from surface oil flow visualization [4] and a recent LES simulation [13].

C. Skewness of p'

It is important to examine the skewness, $S_p = \overline{p'^3}/(\overline{p'^2})^{3/2}$, of the p' probability density function (PDF) in order to understand its behavior on the bump surface. It is well known that the noise-removal method by the subtraction of two microphone signals, which is applied in the present study, does not give the pure third and higher moments of p' due to the turbulence, because this method is limited to the measurement of the power spectrum and rms level of turbulent pressure fluctuations [24]. In other words, the subtraction method does not provide the time series signals of p' due to the turbulent boundary layer. However, the approximate skewness of p' on the bump surface can be estimated from the subtracted time signal as long as it is the linear combination of two independent signals and one is a Gaussian distribution for which the third moment is equal to zero, with a much lower variance than the other. Assuming the two independent random variables A and B with μ_3 of the third moment about the mean μ and σ of the standard deviation, respectively, the skewness of the $A + B$ variable is able to be approximated by Eq. (2) if B has a normal distribution with much smaller $\sigma(B)$ than $\sigma(A)$:

$$S_{A+B} = \frac{\mu_3(A+B)}{\sigma^3(A+B)} = \frac{\mu_3(A)+\mu_3(B)}{\sigma^3(A)+\sigma^3(B)} \approx \frac{\mu_3(A)}{\sigma^3(A)} \tag{2}$$

The subtracted p' signal consists of a large p'_{1t} on the bump surface and a much smaller p'_{2t} on the flat plate, spanwise apart from p'_{1t}. The p'_{1t} and p'_{2t} are due to the local turbulence at each location and are not correlated down to $f \approx 40$ Hz ($2\pi f\delta/u_\tau \approx 10$), as shown in Fig. 3. The skewness of subtracted signals is equal to the sum of each third moment divided by the sum of the 3/2 power of each variances. Furthermore, the p'_{2t} PDF on the flat plate is very similar to that of a 2DTBL because it is not affected much by the presence of the bump, and its variance is much smaller than that for p'_{1t} on the bump surface. Gravante et al. [21] measured the skewness and kurtosis, $\overline{p'^4}/(\overline{p'^2})^2$, of a 2DTBL p' to be zero and 4.5, respectively, up to $Re_\theta = 7,076$. It is symmetric but not Gaussian. They suggested that the negative skewness S_p reported by Schewe [25] and Karangelen [26] is due to the spatial averaging effect of pinhole diameters on the tails of the p' PDF. Therefore, it is reasonable to approximate the skewness of subtracted signals to be close to that for p' due to the turbulence on the bump surface.

It is useful to discuss the skewness S_P with the intermittency of local U_L, which is the time fraction of positive velocity in local coordinates. Figure 6a shows the contours of the intermittency of local U_L. It shows a wide spatial region on the leeside, where the instantaneous local backflow and the large intermittent attached and detached flow occur as mentioned earlier. Figure 6b shows the contours of the skewness S_P of the p' PDF on the leeside, with positive values downstream from the bump apex and near zero as the locations move downstream. It is negatively skewed in the mean backflow region. The positive skewness in the upstream region may be due to the intermittent large amplitude negative u' produced by the large eddies, driving the low-velocity fluid away from the wall [7]. Another way to look at this is that, as the flow remains attached over a greater leeside region infrequently, the flow also decelerates more with an increase in local pressure infrequently. The skewness changes sign from positive to negative through the high adverse pressure gradient region between incipient detachment (ID) and ITD along the centerline (Fig. 4). The negative skewed p' features in the mean backflow separated region indicate very infrequent low instantaneous pressure and infrequently occurring large backflow zones that extend far upstream ($x/H < 1$). It also may be due to large-scale eddies above $y^+_{L0} \approx 100$ and the outer layer, because the mean shear and TKE levels are low in the mean backflow region, below $y^+_{L0} \approx 100$ [6]. There are no bimodal histograms of p' observed on the bump leeside, in spite of the bimodal velocity histogram features of u'_L and w'_L [6].

D. Surface-Pressure Fluctuation Spectra and Their Contributions to $\overline{p'^2}$

The turbulence over the bump leeside features highly unsteady 3-D separations and low-frequency large eddies associated with the streamwise vortices that emanate from the separations. The characteristics of surface-pressure fluctuation spectra are examined in relation to the turbulence structure over the bump.

Figure 7 shows the normalized PSD of p' along the centerline versus a nondimensional as well as a dimensional frequency. As expected, because of the unsteady bimodal leeside separation, there are very high spectral levels in the low-frequency region that are larger on the leeside than the windward side. On the windward side, shown in Fig. 7a, the spectral levels below $St \approx 1$ vary about as $f^{-0.5} \sim f^{-1}$ and as f^{-5} in the highest frequency region, which is typical for a 2DTBL in accelerating flow regions [16]. It is noted that the spectral levels in $1 < St < 10$ show about f^{-2} decay before the f^{-5} dependence appears. It is probably due to the sources in the buffer zone in the boundary layer, as Olivero-Bally et al. [27] and Gravante et al. [21] reported an $f^{-7/3}$ dependence in their p' spectra for zero pressure gradient, flat plate, fully turbulent boundary layers.

Downstream of the bump apex, the high spectral levels for $St < 0.1$ at $x/H = 0.254$ in Fig. 7b vary about as f^{-3} until an f^{-5} dependence appears. When compared with the p' PSD at $x/H = -0.254$ in Fig. 7a, the spectra at $x/H = 0.254$ is higher at low frequencies due to the adverse pressure gradient and larger v' near the wall. For $x/H = 0.254$, a more constant spectral level for $3 < St < 7$ is observed before a f^{-5} decay, which is also observed at other x/H locations downstream in Fig. 7b. The frequency range of the flat spectral level decreases as x/H approaches the separation location. This is a significant feature of surface-pressure fluctuation spectra

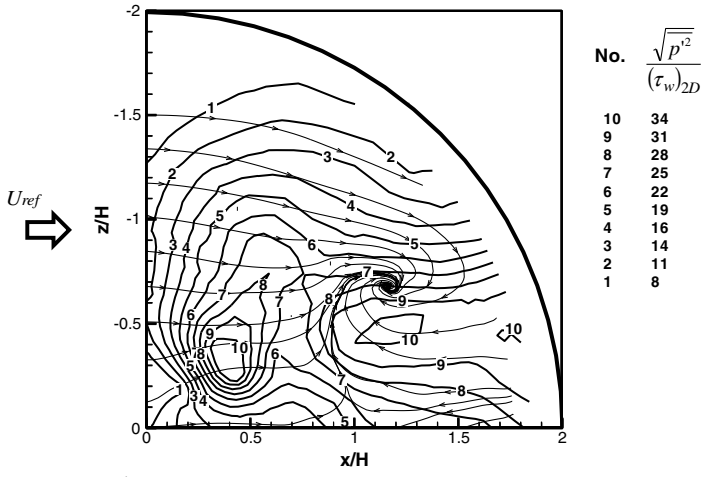

Fig. 5 Numbered contours of normalized p' rms on the bump leeside. Thin solid lines denote the near-wall mean flow pattern at $y^+_{L0} = 6$ [6].

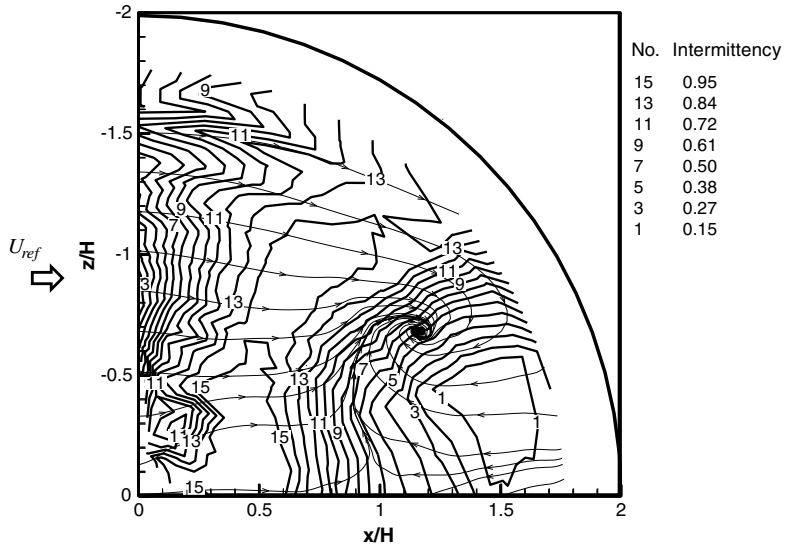

a) Intermittency of local U_L [7]

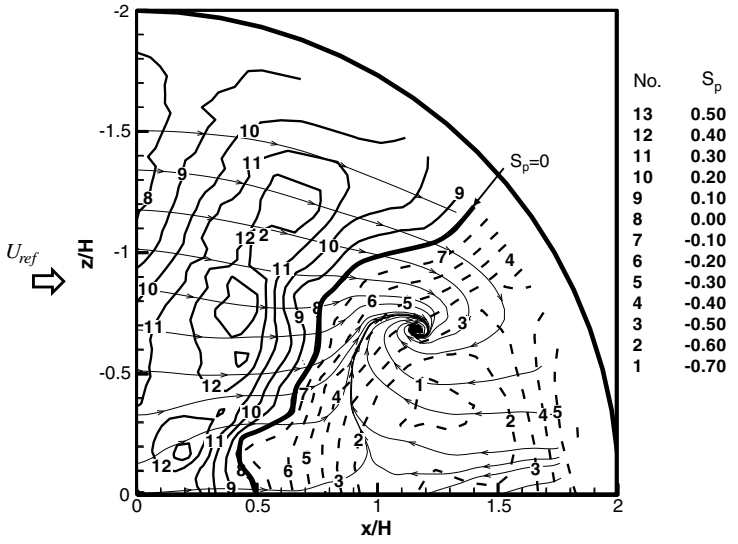

b) Skewness of p'

Fig. 6 Intermittency contour and approximate skewness S_p contour of p' PDF on the bump leeside. Dashed lines denote negative values. Thin solid lines denote the near-wall mean flow pattern at $y^+_{L0} = 6$ [6].

observed beneath the 3-D turbulent boundary layer and results from the lack of overlapping structure between the large-scale outer-layer and fine-scale near-wall-pressure generating motions and from the considerable increase of the spectral level in high frequencies [2,3]. These frequency regions of flat spectral level play dominant contributions to $\overline{p'^2}$ in the premultiplied spectrum (Φf), shown in Fig. 8. Returning to Fig. 7c, the spectra downstream of the saddle separation collapse fairly well, implying similar pressure-generating sources in this region. For all x/H locations, a decay varying like $f^{-7/3} \sim f^{-3}$ appears for $St > 0.3$, and the spectral humps exist at around 30 and 100 Hz.

Figure 8 shows the premultiplied PSD of p' along the centerline. It indicates the major frequency ranges contributing to $\overline{p'^2}$. As expected, it shows a much lower power level over the spectrum on the windward side and that there are large low-frequency contributions to generate p' on the leeside bump surface. There are two peaks in the premultiplied PSD. The first peak appears at $f \approx 30$ Hz for most leeside locations. The second peak appears at $f > 90$ Hz, and the peak frequency decreases as x/H increases, while the corresponding premultiplied PSD level increases. It is probably associated with increasing dominant source scales along the centerline.

To examine the PSD variation of surface-pressure fluctuation off the centerline, the PSD and premultiplied PSD for $r/H = 1.386$ are shown in Fig. 9. Note that an r/H is equal to an x/H for $\psi = 0°$, and the focus is located at $\psi = 30°$ along $r/H = 1.386$, as shown in Fig. 1a. The spectra collapse well for $\psi \leq 40°$ from $St \geq 0.7$. In the low-frequency region, the higher spectral level and their contributions to $\overline{p'^2}$ appear at $\psi = 10$ and 20° due to higher v' in the outer layer associated with the streamwise vortices emanating from the separation lines upstream. The spectral levels for $\psi = 50$ and 60° in the $0.07 \leq St \leq 0.4$ range are much lower, resulting in much lower contributions to $\overline{p'^2}$. The frequency for the second peak in the premultiplied PSD increases as ψ increases from the focus ($\psi \geq 30°$), while it does not change much near the centerline ($\psi < 30°$). It shows a different trend from that observed in Fig. 8b, implying not much change of pressure-generating velocity eddy scales corresponding to this second peak frequency range between the centerline and the focus. The contribution of low-frequency contents to $\overline{p'^2}$ on the bump leeside is more than 55% for $f < 50$ Hz and 64% for $f < 100$ Hz.

The cross-spectral features of the p' on the bump leeside are shown in Fig. 10. The coherence function γ^2 is obtained from the cross

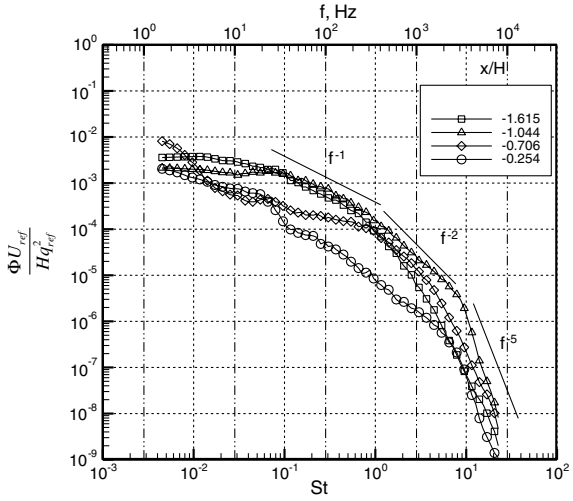

a) Windward side

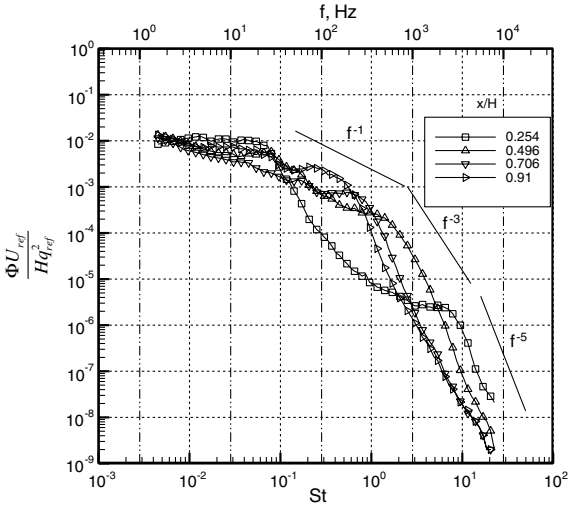

b) Leeside, upstream from separation

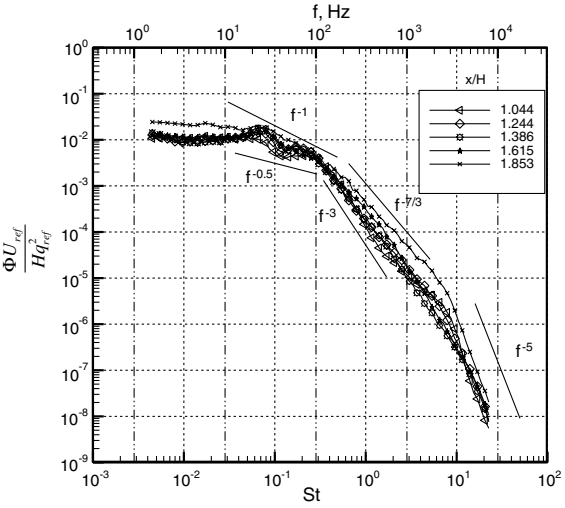

c) Leeside, downstream from separation

Fig. 7 Power spectral density of p' along the centerline.

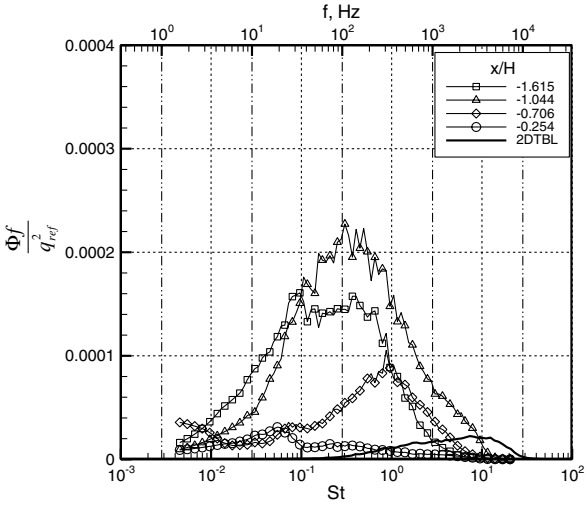

a) Windward side

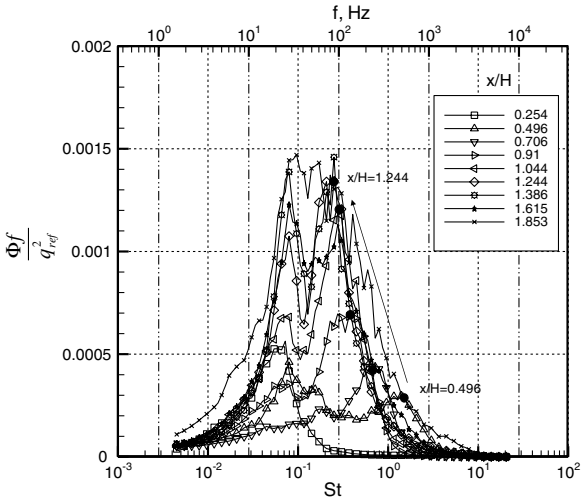

b) Leeside

Fig. 8 Premultiplied PSD (Φf) of p' along the centerline. $\int_0^\infty \Phi f \, \mathrm{d}[\ell n(f)] = \overline{p'^2}$. Filled circles indicate second peak levels from $x/H = 0.496$ (bottom) to $x/H = 1.244$ (top).

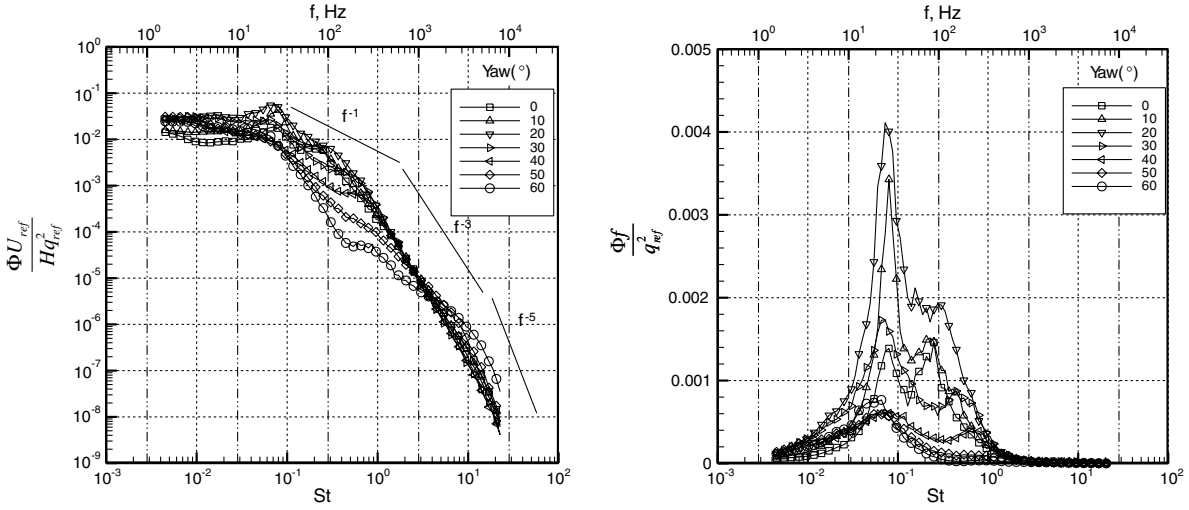

a) PSD of p' **b) Premultiplied PSD (Φ*f*) of p'**

Fig. 9 Power spectra of p' at $r/H = 1.386$.

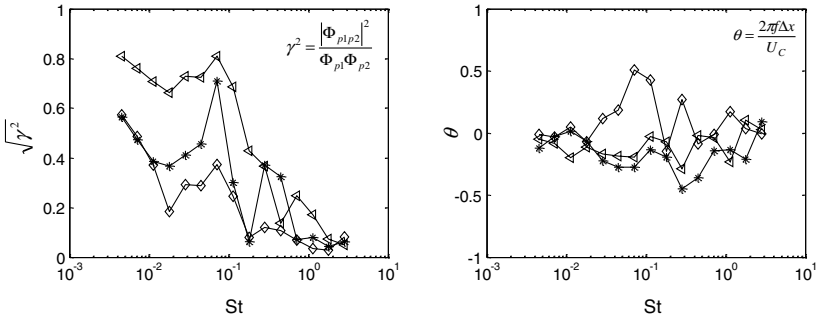

a) Coherence function **b) Phase angle (rad)**

Fig. 10 Coherence function of p' along the centerline. p'_1 at $x/H = 1.615$ and p'_2 at $x/H = 0.706$ (◇), 1.244 (*), and 1.386 (◁).

spectrum of p' for two microphones mounted on the leeside surface along the centerline with a streamwise separation. One is located at $x/H = 1.615$ and the other along the centerline in order to examine the pressure field coherent features upstream and downstream of the separation location. Note that the noise-cancellation technique is not applied to these calculations. Although the noise effects are included, the coherence functions show a pressure fluctuation behavior with Δx as a function of frequency. The very high coherence and the negative phase differences are observed below $St \approx 0.1$, downstream of the separation location. This is the supporting evidence that the large-scale eddies are a dominant source of surface-pressure fluctuations in the separated region. It should be mentioned that Ma and Simpson [28] reported most Reynolds stresses are generated by the turbulent motions below 34 Hz ($St \approx 0.1$) in the near wake downstream, which is very close to the peak frequency in Fig. 10a. However, they did not show a spectral peak corresponding to $St \approx 0.1$. In spite of the peak coherence near $St \approx 0.1$, the large-scaled coherent vortex-shedding process should be associated with the very low-frequency range of meandering motions over the bump leeside instead of one peak frequency [7,13]. It may mean the different time scale of the shedding process from the cylinder. Byun [7] showed very high coherence of surface tangent velocities for $f < 30$ Hz, which is corresponding to the bimodal PDF of U_L and W_L. The analysis of bimodal velocity structure results in the separation of attached and detached flow modes on the leeside. From the detached mode, the saddle-focus separation meanders on the wide region of the leeside.

The convection velocity U_c is calculated using the phase angle (Fig. 10b). Note that U_c is an average value for $0.018 \leq St \leq 0.07$, where the coherence is greater than 0.2. For upstream from the separation ($\Delta x/H = 0.91$ and $x/H = 0.706$ and 1.615), the U_c is about $0.54U_{\text{ref}}$, implying the pressure field associated to large-scaled eddy structures, emanated from 3-D separations, is convected downstream with these structures. For downstream from the separation ($\Delta x/H = 0.37$, $x/H = 1.244$ and 1.615, $\Delta x/H = 0.23$, and $x/H = 1.386$ and 1.615), however, the convection velocities are $-0.48U_{\text{ref}}$ and $-0.34U_{\text{ref}}$, indicating that the pressure field is convected upstream, with large-scaled eddy structures in the mean backflow region.

IV. Conclusions

The characteristics of surface-pressure fluctuations are investigated for the separated flow over a smoothly contoured axisymmetric bump. The approaching 2-D turbulent boundary layer has the momentum thickness Reynolds number of $Re_\theta = 7300$ and the boundary-layer thickness δ of half of the bump height. The flow over the bump is characterized by highly unsteady saddle-focus separations on the leeside-curved surface, resulting in large-scaled dominant turbulent structures with a low frequency.

The rms value of p' decreases on the windward side and begins to increase over the bump top. It reaches the local maximum near the reattachment region near the downstream edge of the bump. From the PSD of p', the spectral levels are high in the low-frequency region, and they contribute dominantly to the resulting $\overline{p'^2}$ on the leeside. In the separated region, large-scaled eddy structures that are associated with the streamwise vortices that emanate from 3-D separations [7] are the major source for the surface-pressure fluctuation from outer layers. Since the p' spectral level is very much higher for this separated flow at low frequencies than other unseparated flows, and the separation vortices are the dominant features, they must be the source of this higher p'. Near the wall, low-velocity gradients in the

backflow region produce low-level high-frequency pressure fluctuation contributions. A highly 3-D flow above a given surface location originates from various upstream regions and shows no equilibrium and overlap region of near-wall and outer layer velocity structures in the separated region [6,7]. Thus, a rapid pressure fluctuation spectral decay from the high level low-frequency content is observed due to the lack of overlapping between large-scaled and finer-scaled motions near the wall in the mean backflow region downstream from the separation. Near the bump apex, the spectral levels are high in the higher frequency region due to the accelerated thinner boundary layer with the high mean velocity gradient and skin friction velocity. From an approximate analysis, the asymmetric negative skewed histogram of surface-pressure fluctuations appears in the separated region. However, the bimodal histogram of surface tangential velocity components is not directly related to the pressure fluctuation histogram.

The flow over a 3-D curved surface is of interest for engineering applications, and there are efforts for CFD researchers to capture the turbulent flow features and the sources of flow-induced noise over this surface. Therefore, the previous flowfield and current surface-pressure fluctuation results for this axisymmetric bump form a useful test case for validating the simulation of surface-pressure fluctuations for highly unsteady 3-D separated turbulent flowfields.

Acknowledgment

This work was supported by the U.S. Office of Naval Research under N00014-07-1-0612, with Ron Joslin as Program Manager.

References

[1] Bull, M. K., "Wall-Pressure Fluctuations Beneath Turbulent Boundary Layers: Some Reflections of Forty Years of Research," *Journal of Sound and Vibration*, Vol. 190, No. 3, 1996, pp. 299–315. doi:10.1006/jsvi.1996.0066

[2] Goody, M. C., and Simpson, R. L., "Surface Pressure Fluctuations Beneath Two- and Three-Dimensional Turbulent Boundary Layers," *AIAA Journal*, Vol. 38, No. 10, 2000, pp. 1822–1831. doi:10.2514/2.863

[3] Goody, M. C., Simpson, R. L., and Chesnakas, C. J., "Separated Flow Surface Pressure Fluctuations and Pressure-Velocity Correlations on Prolate Spheriod," *AIAA Journal*, Vol. 38, No. 2, 2000, pp. 266–274. doi:10.2514/2.953

[4] Simpson, R. L., Long, C. H., and Byun, G., "Study of Vortical Separation from an Axisymmetric Hill," *International Journal of Heat and Fluid Flow*, Vol. 23, No. 5, 2002, pp. 582–591. doi:10.1016/S0142-727X(02)00154-6

[5] Byun, G., Simpson, R. L., and Long, C. H., "Study of Vortical Separation from Three-Dimensional Symmetric Bumps," *AIAA Journal*, Vol. 42, No. 4, 2004, pp. 754–765. doi:10.2514/1.1829

[6] Byun, G., and Simpson, R. L., "Structure of Three-Dimensional Separated Flow on an Axisymmetric Bump," *AIAA Journal*, Vol. 44, No. 5, 2006, pp. 999–1008. doi:10.2514/1.17002

[7] Byun, G., "Structure of Three-Dimensional Separated Flow on Symmetric Bumps," Ph.D. Dissertation, Department of Aerospace and Ocean Engineering, Virginia Polytechnic Inst. and State Univ., Blacksburg, VA., 2005.

[8] Temmerman, L., Wang, C., and Leschziner, M. A., "A Comparative Study of Separation from a Three-Dimensional Hill Using LES and Second-Moment-Closure RANS Modeling," *European Congress on Computational Methods in Applied Sciences and Engineering*, July 2004.

[9] Wang, C., Jang, Y. J., and Leschziner, M. A., "Modelling Two-and Three-Dimensional Separation from Curved Surfaces with Anisotropy-Resolving Turbulence Closures," *International Journal of Heat and Fluid Flow*, Vol. 25, No. 3, 2004, pp. 499–512. doi:10.1016/j.ijheatfluidflow.2004.02.009

[10] Davidson, L., and Dahlström, S., "Hybrid LES-RANS: Computation of the Flow Around a Three-Dimensional Hill," *Engineering Turbulence Modeling and Experiments*, Vol. 6, Elsevier, New York, 2005, pp. 319–328.

[11] Persson, T., Liefvendahl, M., Bensow, R. E., and Fureby, C., "Numerical Investigation of the Flow Over an Axisymmetric Hill Using LES, DES, and RANS," *Journal of Turbulence* [online journal], Vol. 7, No. 4, 2006, http://www.informaworld.com/smpp/content~content=a758811182 [retrieved 2 June 2010]. doi:10.1080/14685240500543165

[12] Krajnovic, S., "Large Eddy Simulation of the Flow Over a Three-Dimensional Hill," *Flow, Turbulence, and Combustion*, Vol. 81, No. 1, 2008, pp. 189–204. doi:10.1007/s10494-007-9120-4

[13] García-Villalba, M., Li, N., Rodi, W., and Leschziner, M. A., "Large Eddy Simulation of Flow over and Around a Three-Dimensional Axisymmetric Hill," *Journal of Fluid Mechanics*, Vol. 627, 2009, pp. 55–96. doi:10.1017/S0022112008005661

[14] Goody, M. C., "An Experimental Investigation of Pressure Fluctuations in Three-Dimensional Turbulent Boundary Layers," Ph.D. Dissertation, Department of Aerospace and Ocean Engineering, Virginia Polytechnic Inst. and State Univ., Blacksburg, VA, 1999.

[15] Simpson, R. L., Ghodbane, M., and McGrath, B. E., "Surface Pressure Fluctuations in a Separating Turbulent Boundary Layer," *Journal of Fluid Mechanics*, Vol. 177, 1987, pp. 167–186. doi:10.1017/S0022112087000909

[16] McGrath, B. E., and Simpson, R. L., "Some Features of Wall Pressure Fluctuations in Turbulent Boundary Layers with Zero and Favorable Pressure Gradients," NASA CR 4051, 1987.

[17] Corcos, G. M., "Resolution of Pressure in Turbulence," *Journal of the Acoustical Society of America*, Vol. 35, No. 2, 1963, pp. 192–199. doi:10.1121/1.1918431

[18] Kline, S. J., and McClintock, F. A., "Describing Uncertainties in Single Sample Experiments," *Mechanical Engineering*, Vol. 75, 1953, pp. 3–8.

[19] Bradshaw, P., "Inactive Motion and Pressure Fluctuations in Turbulent Boundary Layers," *Journal of Fluid Mechanics*, Vol. 30, No. 2, 1967, pp. 241–258. doi:10.1017/S0022112067001417

[20] Blake, W. K., "Turbulent Boundary Layer Wall Pressure Fluctuations on Smooth and Rough Walls," *Journal of Fluid Mechanics*, Vol. 44, No. 4, 1970, pp. 637–660. doi:10.1017/S0022112070002069

[21] Gravante, S. P., Naguib, A. M., Wark, C. E., and Nagib, H. M., "Characterization of the Pressure Fluctuations Under a Fully Developed Turbulent Boundary Layer," *AIAA Journal*, Vol. 36, No. 10, 1998, pp. 1808–1816. doi:10.2514/2.296

[22] Goody, M., "Empirical Spectral Model of Surface Pressure Fluctuations," *AIAA Journal*, Vol. 42, No. 9, 2004, pp. 1788–1794. doi:10.2514/1.9433

[23] Simpson, R. L., "Turbulent Boundary Layer Separation," *Annual Review of Fluid Mechanics*, Vol. 21, No. 1, 1989, pp. 205–234. doi:10.1146/annurev.fl.21.010189.001225

[24] Naguib, A. M., Gravante, S. P., and Wark, C. E., "Extraction of Turbulent Wall-Pressure Time-Series Using an Optimal Filtering Scheme," *Experiments in Fluids*, Vol. 22, No. 1, 1996, pp. 14–22. doi:10.1007/BF01893301

[25] Schewe, G., "On the Structure and Resolution of Wall-Pressure Fluctuation Associated with Turbulent Boundary Layer Flow," *Journal of Fluid Mechanics*, Vol. 134, 1983, pp. 311–328. doi:10.1017/S0022112083003389

[26] Karangelen, C. C., "Temporal and Spectral Features of Wall-Pressure Fluctuations Beneath a Turbulent Boundary Layer," Ph.D. Thesis, Catholic Univ. of America, Washington, DC, 1991.

[27] Olivero-Bally, P., Forestier, B. E., Focquenoy, E., and Olivero, P., "Wall Pressure Fluctuations in Natural and Manipulated Turbulent Boundary Layers in Air and Water," *FED/Flow Noise Modeling, Measurement and Control*, Vol. 168, American Society of Mechanical Engineers, New York, 1993.

[28] Ma, R., and Simpson, R. L., "Characterization of Turbulent Flow Downstream of a Three-Dimensional Axisymmetric Bump," *4th International Symposium on Turbulence and Shear Flow Phenomena*, Williamsburg, VA, 27–29 June 2005, pp. 1171–1176.

J. Gore
Associate Editor